Reply to the comments from anonymous referee#2:

We sincerely thank referee#2 for the valuable feedback that we have used to improve the quality of our manuscript. The referee's comments are laid out in *italicized font* and the comments have been numbered in the authors' responses. Our responses are given in normal font and changes/additions to the manuscript according to referee#2 are given in red text (blue texts are revisions according to referee#1, some of the revisions can also be considered as responses to referee#2's comments). The authors' responses and the revised manuscript can be found in the attachment.

Sincerely Yours,
Dr. Jiang Xingjie

Authors' Responses:

This manuscript aims at providing a systematic approach that allows a convenient and quantitative comparison of non-Gaussianity of real-world wave fields through the corresponding wave spectra. The newly proposed approach includes: i) a set of pre-calculated references representing the relation of non-Gaussianity to spectral geometries, and ii) an approach to introduce arbitrary 2D spectra into the references. Since the occurrence of rogue waves is closely related to the two issues: spectral geometries and non-Gaussianity of sea states, we applied this approach to some rogue events occurred in real oceans. The results confirmed with the existing theories and conclusions, and provided a quantitative support regarding the topic of "explaining formation of rogue waves without modulational instabilities" in wind-sea dominated sea states. Apparently, the newly proposed approach is operational and can be used in more studies related to rogue wave sea states.

Comment 1: *I have doubts about the negative values of kurtosis for rather small directional spreading. It could be seen from Fig. 3(c,d) that the negative values of kurtosis are observed for small wave steepness (looking at the figure, I cannot estimate the kurtosis value for larger ε). I think this may be due to insufficient statistics of waves for the initial conditions, when a Gaussian field is constructed. ... Secondly, such negative values might be a result of the high-frequency cut-off. ...*
Response: Negative values of $R_{\mu 4}$ come from the negative average $\overline{\mu_4}$, see Eq. (8) in Sect. 2.3. The four panels shown in Fig. 1 below illustrate μ_4 time series obtained (averaged from 80 repetitions) with some of the initial conditions in the HOSM simulations. The combination of $(\varepsilon, \gamma, \Theta)$ for each initial condition is presented in the upper-right corner of each panel, together with the value of $\overline{\mu_4}$. One of the explanations for negative $\overline{\mu_4}$ is: it can be seen in Fig. 1 that, these time series of μ_4 oscillate slightly and randomly near the level of 0 (rather than always below the 0 line), resulting in the average $\overline{\mu_4}$ being less than 0. On the other hand, as the lines labeled '0' shown in Fig. 2, negative values of $R_{\mu 4}$ all appear when the spectral parameter ε is very small, most of them appear when $\varepsilon = 0.01$ and a small amount appear at $\varepsilon = 0.02$; and if ε is small, negative $R_{\mu 4}$ concentrates primarily in the range of $\Theta < 120$, although they can appear at any position within the scope of γ. Thus, another explanation for negative $\overline{\mu_4}$ might be: as introduced in Sect.1, the simulated time series of μ_4 represents the contributions from both free μ_4^{free} and bound μ_4^{bound} waves, and μ_4^{free} may get negative values as the special ratio of BW to DS appears, resulting a defocusing of wave energy in such a wave field, see Fig. 1 of Fedele (2015); however, μ_4^{bound} is always positive and proportional to ε (Janssen, 2009). Therefore, if ε is so small that μ_4^{bound} cannot offset a negative value of μ_4^{free}, the total kurtosis may get a negative value; such a situation can be alleviated as ε increases, thus, negative kurtosis cannot be found with larger ε in Fig. 2.

In the HOSM simulations, the number of waves involved in each initial wave field was almost the same, i.e., 25.5x25.5 waves as mentioned in Sect. 2.1. The negative kurtosis seems unlikely to be caused by the insufficient statistics of waves, since most of the kurtosis obtained were positive under initial conditions with same wave numbers. On the other hand, in each of the HOSM simulations, the cut-off frequency was set at $k_{max} = 5k_p$, where k_p denotes the peak wavenumber/frequency of the initial spectrum. Such a cut-off frequency may allow accurate solution of the most energetic part of the spectrum and restrict the breaking of waves in the wave field to within a very limited level (Ducrozet et al., 2017). And it should be noted that, the $5k_p$ cut-off frequency adopted in the HOSM simulations were not fixed values but automatically adapted according to the

initial spectra. Again, since the kurtosis obtained was not always negative under similar experimental environments, the negative kurtosis seems unlikely to be caused by the cut-off frequency.

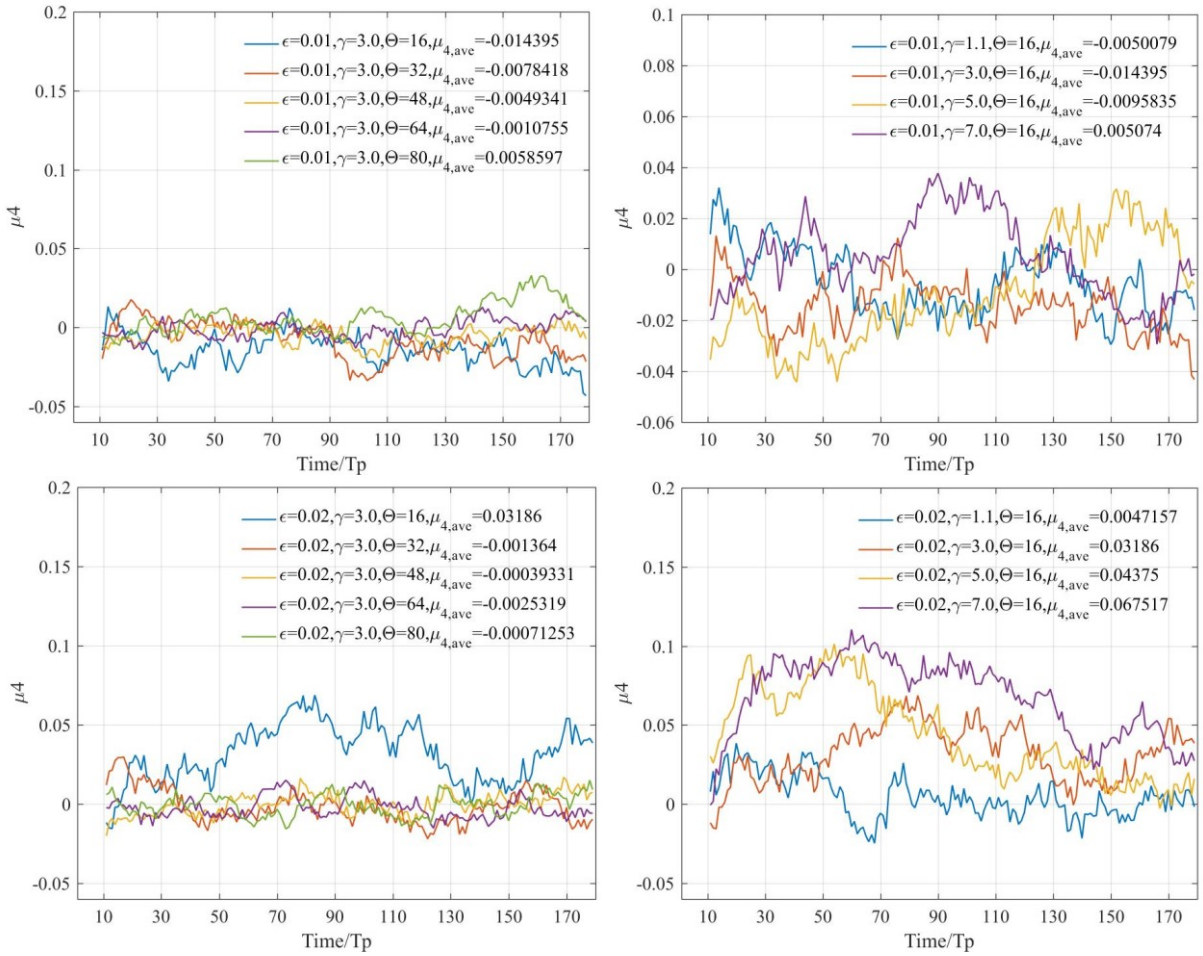

Fig. 1 μ_4 time series obtained in some of the HOSM simulations

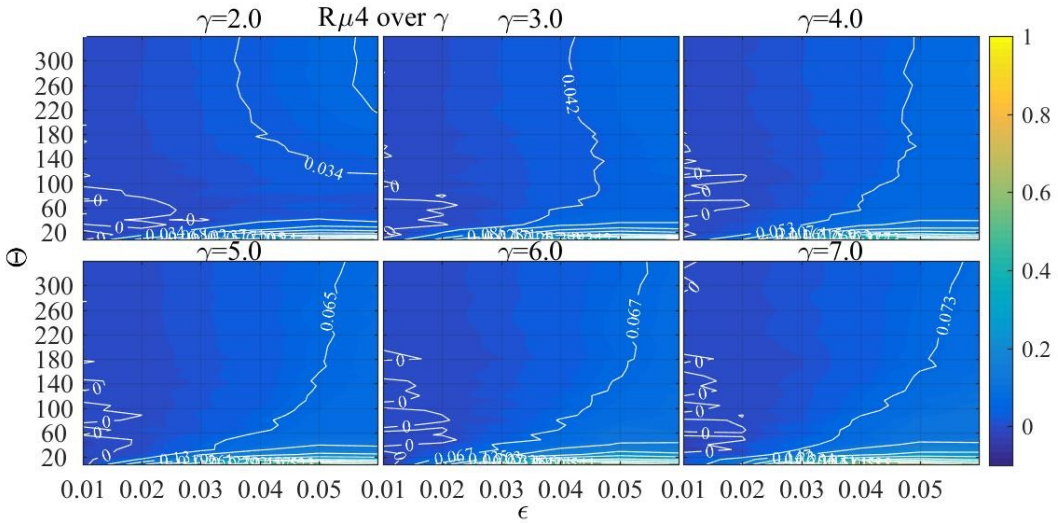

Fig. 2 $R_{\mu 4(\varepsilon,\Theta)}$ with discrete γ within 2.0-7.0

And those negative $R_{\mu 4}$ would not influence identification of $(\varepsilon, \gamma, \Theta)$ combinations that can trigger rogue waves, see the response to Comment 14 below.

Comment 2: *In the numerical experiments by HOSM (section 2.1), the spatial sampling was about 10 points per a wavelength. To the best of my knowledge, it is not sufficient to describe accurately the wave features, what may lead to artifacts of processing.*

Response: We understand that the description of the wave surface would be more accurate if finer spatial resolution was adopted. However, the purpose of the HOSM simulations was to obtain the statistical skewness and kurtosis of the entire simulated wave fields, rather than to get the wavefront information of a particular wave. Therefore, we thought lower spatial

resolution could also be accepted. Similar spatial resolution settings can also be found in Durcrozet et al. (2016, 2017).

In fact, the spatial resolution is closely related to the cut-off frequency and the maximum wave steepness ($\varepsilon = H_s/\lambda_p$) allowed in the HOSM simulations. As mentioned in Sect.2.1, the relation between the cut-off frequency k_{max} and the spatial resolution is

$$k_{max} = \frac{\mathrm{N}-1}{2} \times \Delta\mathrm{k} = \frac{\mathrm{N}-1}{2} \times \frac{2\pi}{nlen \times \lambda_p} = nlen \cdot \frac{\mathrm{N}-1}{2} \times k_p,$$

where $nlen$ is the number of wave length considered in the simulated wave fields, N is the number of grid points in the physical space, and k_p is the peak frequency of each initial spectrum. According to Ducrozet et al. (2017), a typical setting of $k_{max} \leq 5k_p$ may allowed an ε up to 0.06 to occur in the simulated wave field (deep water case). Though larger $nlen$ or larger N in the equation above may lead to a finer spatial resolution, the simulation cannot be maintained when large wave steepness occurs (the steep wave might break, and the HOSM simulation could not deal with such an issue). Since ε up to 0.06 can be observed in real sea states (see Fig. 1 of the manuscript), the spatial resolution and the cut-off frequency were set to let the simulations could be done with occurrence of such extremely large wave steepness. On the other hand, smaller $nlen$ and larger N can also maintain the same cut-off frequency, but the resolution of the related pseudo-spectral space $\Delta\mathrm{k} = \frac{1}{nlen} k_p$ might become too loose to lead to another kind of artifacts in the evolution of the spectra simulated. Details of the pseudo-spectral space can be found in the response to Comment 8.

Comment 3: *The statistical moments are calculated by averaging over a remarkably long period of 170 after the start of the simulation. … Therefore the averaging over 170 wave periods will most likely completely hide the effects of the modulational instability. … Anyway, it would be instructive if the maximum attained values of skewness and kurtosis for the given spectral parameters are plotted in e.g. Fig. 8,9 in line with the averaged ones.*

Response: For some initial spectra with larger steepness, and narrower band and directional width, the evolution of μ_3 and μ_4 time series might become insignificant after $130 - 150T_p$, see Fig. 3 below. And we extended the statistical moments up to $180T_p$ to include all the process. On the other hand, initial spectra with lower steepness, and broader frequency and directional distribution might be related to μ_3 and μ_4 time series without a clear trend, like the time series shown in Fig. 1. Therefore, maximum values of μ_3 and μ_4 time series might be unsuitable to be adopted as the non-Gaussianity indicators.

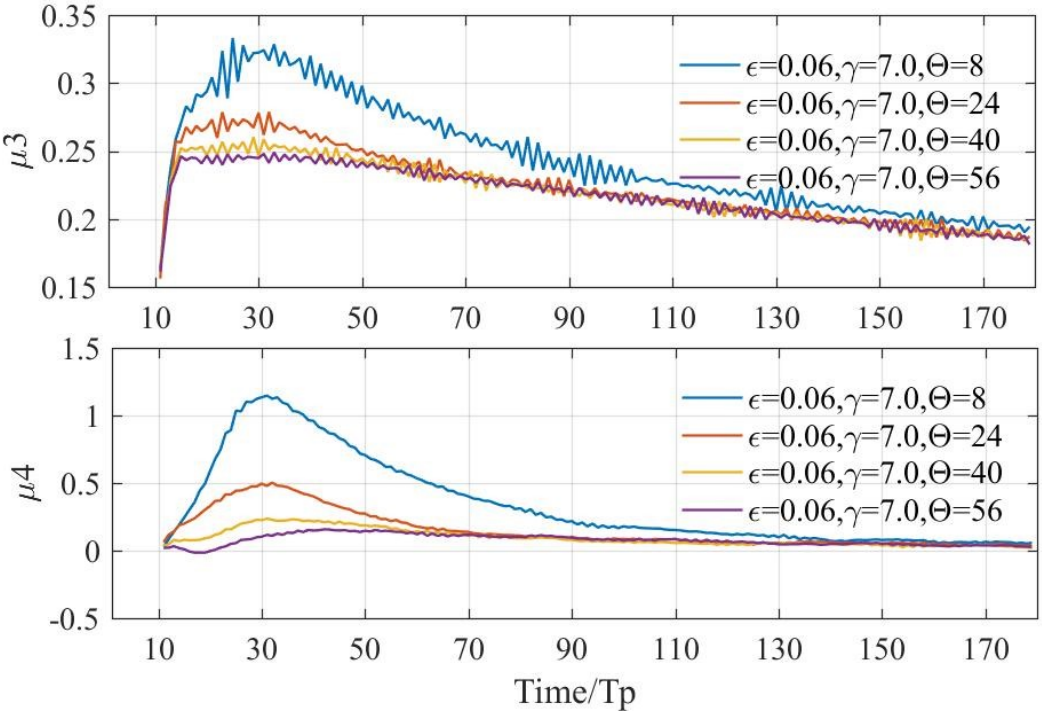

Fig. 3 μ_3 and μ_4 time series for some steeper and narrower initial spectra

Comment 4: *In Sec. 3.2 the values of the skewness and kurtosis which characterize the Draupner wave and the Andrea wave seem to be rather different from the results of a similar analysis performed in [Fedele, F., Brennan, J., Ponce de León, S., Dudley, J. and Dias, F. Real world ocean rogue waves explained without the modulational instability., Sci. Rep., 2016]. Please*

discuss possible reason of this disagreement.
Response: The possible reasons of the disagreement could be different wind force used, different model settings, and so on. In this manuscript, the wave parameters of the simulated sea states have been compared with observed data that digitalized from published research, see Fig. 5 and Table 2–3 in the manuscript. We think observed data is more reliable and convincing, and the goodness of the fit of the simulated and observed parameters is acceptable enough for the following sea state analyses in the manuscript. So, comparison of our results with other simulated results published might be unnecessary according to the aim of this manuscript.

Comment 5: *The work is lacking in discussion and comparison with previously reported results on similar problems, even though the publications are mentioned. In particular, the BFI parameter is not mentioned in the work at all, although it seems to be a most promising characteristic of the extremality of sea states. The in-situ extreme events considered in the article have already been analyzed earlier, but the new results are not discussed against the already reported.*
Response: Similar comment was also given by referee#1, and we have added some discussion and comparison with previously published research, please see the blue texts in the introduction and discussion sections.

The BFI parameter is indeed a very important indicator used to indicated the activity of modulational instabilities (MI), and there are also many kinds of modified BFI that has been proposed to present the influence of directional spreading on MI, e.g., Xiao et al. (2013), Waseda et al. (2009). However, as mentioned in the introduction and discussion sections (blue texts) of the revised manuscript, those indicators might be not suitable to be used to estimate the non-Gaussianity and its relation to spectral geometries in real sea states, because: i) the original expression of BFI was derived under ideal assumptions of narrowband and unidirectionality, when applying them to the real sea conditions, specific and undetermined parameters were involved, and those parameters were not calibrated according to the skewness/kurtosis observed in real sea states, since it is impossible to accurately estimate the number of waves involved in the statistical process; and ii) though there were modified BFI parameters derived base on spectrum models that conform to the characteristics of real wave environment, there is still a lack of way to introduce arbitrary 2D wave spectra into such models. Therefore, if those BFI parameters were adopted to be compared with the newly proposed non-Gaussianity indicators, we could not tell whether the undetermined parameters or the introducing approach used were proper, and those factors might influence the value of those BFI parameters significantly.

The purpose of this manuscript is to present the new approach that allows a comparison of non-Gaussianity of sea states through the corresponding 2D wave spectra, the in-situ extreme events introduced in this manuscript was i) to show the operational feasibility of the newly proposed approach, and ii) to illustrate the relation of sea state non-Gaussianity to spectral geometries in these events. However, previously published related research paid more attention to the characteristics of these extreme events, and rarely discussed the relation. Focusing on the topic of non-Gaussianity and spectral geometries in these extreme events, our conclusions have been discussed in comparison with Fedele et al. (2016) in the revised manuscript.

Comment 6: *The text is generally not easy-to-read due to the numerous notations, which are not always obvious.*
Response: We will seriously consider this comment.

Comment 7: *What is "a relevant parameter n=4"?*
Response: Numerical instabilities may arise from fully nonlinear computations that start with linear initial conditions (Dommermuth, 2000). In order to overcome this problem, Dommermuth (2000) introduced a relaxation scheme, allowing a smooth transition from linear initial conditions to fully nonlinear computation. Two parameters $T_a = 10$ and $n = 4$ were included in the scheme, where $T_a = 10$ denotes a relaxation period of $10T_p$. The parameters T_a and n were set just to ensure the stability of the calculation, and the settings would not affect the results simulated. Since the first $10T_p$ wave fields simulated should be removed from the statistical process to avoid the influence of the relaxation scheme on skewness/kurtosis calculated, we kept the introduction about the relaxation period and deleted the words of *"a relevant parameter n=4"* to avoid ambiguous understandings, see Line 115 in the revised manuscript.

Comment 8: *Please clarify what "pseudo-spectra" means? The same question about "pseudo-spectral space" in Table 1.*

Response: To solve the numerical integration of the potential Euler equations mentioned in Sect. 2.1, the pseudo-spectral method was adopted. Here, the pseudo-spectral method means certain operators (in the equations presented in Sect. 2.1) including the nonlinear terms are treated in the physical space instead of the spectral space. This is necessary to solve the nonlinear terms by avoiding convolution integral in the frequency domain. The transforms between the physical and spectral spaces are handled efficiently using fast Fourier transforms. Thus, the size and resolution of a pseudo-spectral space is highly related to the physical space simulated. Most of the HOS models including the HOS-Ocean used in this study are all pseudo-spectral methods, details could be found West et al. (1987), Dommermuth and Yue (1987), Ducrozet et al.(2016) and other HOSM related references.

Comment 9: *In Eq. (4) should be β instead of B.*

Response: We need to admit that the character "*β*" was missing in the expression $\boldsymbol{\beta} = \begin{cases} \sigma_a, f \le f_p \\ \sigma_b, f > f_p \end{cases}$ (Line 139 in the revised manuscript). And the parameter B expressed in Eq. (4) actually is the coefficient that has been presented in Eq. (3).

Comment 10: *The writing cos2x should be probably used in Eq. (5).*

Response: Eq. (5) has been corrected according to your suggestion.

Comment 11: *It should be μ3 in the expression for the skewness, Eq. (8).*

Response: Eq. (8) has been corrected according to your suggestion.

Comment 12: *The surfaces in Figs. 3 are probably not the best way to present the data, since the non-monotonic change of kurtosis is hardly seen. I suggest using contour plots or something similar (the top-view with a color coding, etc.)*

Response: The value of $R_{\mu 4}$ changes greatly when the parameter Θ is extremely narrow. If $R_{\mu 4}$ is demonstrated in a contour plot, the contours will be concentrated in a very narrow range, and outside the range, the contours might be very sparse. An example might be seen is Fig. 2 shown above. So, we prefer the current way to demonstrate $R_{\mu 4}$ as shown in Figs. 3. Moreover, we have decided to open the access of the pre-calculated non-Gaussianity references, readers who are interested can redraw the figures by themselves.

Comment 13: "…in a normal sea state (Annenkov and Shrira, 2014)".Do you mean "Gaussian sea state" or "typical sea state"?

Response: It means " **a sea state with broad band width and directional spreading**", and the statement has been revised in Line 224-225 in the revised manuscript.

Comment 14: *"Negative Rμ4 values represent sea states with less possibility of finding rogue waves; thus, they would not influence identification of MI-triggering combinations." Please explain what you mean.*

Response: We need to admit that this statement described a wrong causality. It should be "**Since negative $R_{\mu 4}$ values represent sea states with inactive MI or defocusing of energy, both factors may lead to less possibility to find rogue waves in such sea states; thus, they would not influence identification of (ε,γ,Θ) combinations that can trigger rogue waves.**", see Line 233-235 in the revised manuscript.

The commonly used measures of the non-Gaussianity of sea states are skewness μ_3 and (excess) kurtosis μ_4 as shown in Eq. (1). As illustrated in Fig. 4 below, probability density function (PDF) with a negative μ_4 (kurtosis<3) may presents thin tails, indicating lower probability of occurrence of extremely high and low surface elevations, i.e., lower probability to find extreme wave heights.

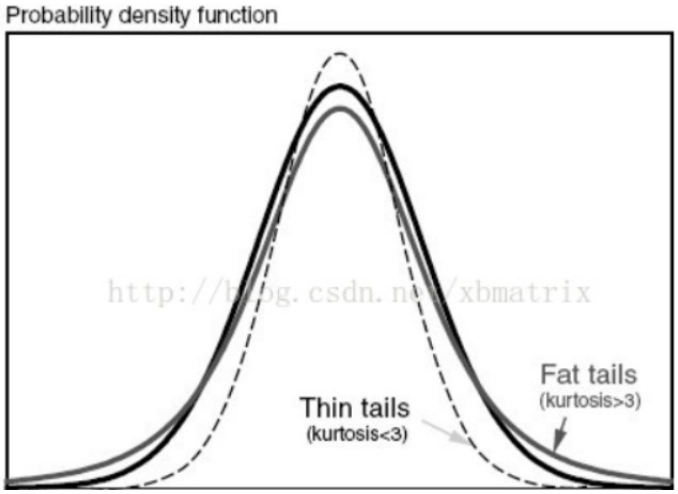

Fig. 4 probability density function with positive and negative kurtosis, the *x*-axis in the figure denotes surface elevations η, where $\eta > 0$ point to the right, $\eta < 0$ point to the left, the *y*-axis denotes the probability for each η occurs; and for a Gaussian distribution, as the thick solid line illustrated in the figure, the peak located at $\eta = 0$.
(this figure is cited from https://blog.csdn.net/qq_36523839/article/details/88671873)

Comment 15: *The subscripts i of the characteristics ε γ Θ are not defined.*
Response: The subscripts i indicate arbitrary position in the scope of ε, γ, and Θ respectively, and the statement has been revised in Line 270-272 of the manuscript.

Comment 16: *"It can be seen from Fig. 7 and Table 3 that the parameters indicating SP are very similar at the times of occurrence of the selected events, i.e., they are almost all within the range of 0.035–0.040." The meaning of the sentence is not clear. Please paraphrase.*
Response: The sentence has been revised as "It can be seen from Fig. 7 and Table 4 that the parameters **s_p and ε_i are almost all within the range of 0.035–0.040 at the times of occurrence of the selected events**" (Line 307-308). Since a new Table 3 was added, the original Table 3 became Table 4 in the revised manuscript.

Comment 17: Tables & Figures
Table 2. Please add to Table 2 the information about Tp and the local water depth.
Response: The local depth has been added to Table 2, and a new Table 3 including the peak period (T_p), peak wavenumber (k_p), and the parameter $k_p d$ (peak wavenumber multiplies the local depth) has also been added. As the blue texts shown at the end of Sect. 3.4 (Line 394-398), the values of parameter $k_p d$ at the times of the occurrences are all greater than the well-known 1.363, indicating that it was not the water depth that restricted the nonlinear focusing caused by MI in the selected events.

Figure 2. The blue colors look similar, therefore the lines are poorly readable. Please change.
Response: Figure 2 has been redrawn, and colored lines with different symbols have been adopted.

Figure 3. Please, swap the figures c) and d) to be consistent with a) and b).
Response: Fig. 3c and Fig.3d have been swapped according to your suggestion.

Figure 4. Please, correct the colorbar (depth, meter). The scale of the depths does not allow to estimate the bathymetry in the vicinity of the locations of measurements. Please indicate the depths of the measurement locations.
Response: Figure 4 has been redrawn, and it is mainly used to illustrates the computational grids. The local depth where the selected events occurred has been listed in Table 2.

Figure 7. The absence of the red curves in the upper panel looks confusing. You could use different line widths or line styles to show the curves which coincide. A new undefined notation Spr appears in the bottom figure. Please change the scale of the left vertical axis – the red lines are poorly read.
Response: Spr in Figure 7 denotes the DS parameter σ_θ (see Eq. (10)), and it has been revised in the redrawn Figure 7. And

in the newly drawn Figure 7, thicker red lines and thinner blue lines were adopted to identify the spectral geometries associated with the non-Gaussianity references and the simulated spectra respectively.

Figure 8. The figure is impossible to read. I can see only two horizontal lines corresponding to the averaged values. I suggest the authors to use different colors and line widths.
Response: Different colors and line-styles have been used to depict $R_{\mu 3}$ and $R_{\mu 4}$ in different events (magenta solid lines for Draupner, blue dotted for Andrea, and red dash-dotted lines for the Alwyn events).

Figure 9. I would expect that the blue dashed lines show the averaged values of the dependences shown with the red curves. However, the plots are inconsistent with this. Could you please explain the relation between the curves in the figure. Please, give the values of Bμ3 and Bμ4 on the graph.
We need to apologize that the additional HOS simulations performed on the Alwyn_r2–Alwyn_r8 events incorrectly used the spectrum of Alwyn_r1 as initial conditions. Therefore, the black and red lines shown in the Alwyn panels in Fig. 9 appear to be at the same level, whereas blue dashed lines were getting lower and lower through Alwyn_r2–Alwyn_r8, conforming to the smaller and smaller values of $R_{\mu 3}$ and $R_{\mu 4}$ shown in Table 3 (Table 4 in the revised manuscript, see the Response to Comment 5 below). And that's why the red lines are obviously larger than the blue ones in all the cases of Alwyn. We sincerely thank referee#1 for pointing out our mistakes. The additional HOS simulations were conducted again on all the 8 Alwyn events with the correct initial conditions, and Fig. 9 was redrawn in the revised manuscript. The newly drawn Fig. 9 proves the inactivity of MI in the Alwyn events, and better goodness of the fit of the blue dashed lines to the red lines can be found in the redrawn figure. The benchmarks $B_{\mu 3} = 0.2753$ and $B_{\mu 4} = 0.6101$, and we think

In Figures 9, 10 the axis tick labels are too dense and even overlap
Response: Figures 9 and 10 has been redrawn according to your suggestion.

Reference:

Dommermuth, D.: The initialization of nonlinear waves using an adjustment scheme, Wave Motion, 32(4), 307–317, doi:10.1016/S0165-2125(00)00047-0, 2000.

Dommermuth, D. G. and Yue, D. K. P.: A high-order spectral method for the study of nonlinear gravity waves, J. Fluid Mech., 184(1), 267, doi:10.1017/S002211208700288X, 1987.

Ducrozet, G., Bonnefoy, F., Le Touzé, D. and Ferrant, P.: HOS-ocean: Open-source solver for nonlinear waves in open ocean based on High-Order Spectral method, Comput. Phys. Commun., 203, 245–254, doi:10.1016/j.cpc.2016.02.017, 2016.

Ducrozet, G., Bonnefoy, F. and Perignon, Y.: Applicability and limitations of highly non-linear potential flow solvers in the context of water waves, Ocean Eng., 142, 233–244, doi:10.1016/j.oceaneng.2017.07.003, 2017.

Fedele, F.: On the kurtosis of deep-water gravity waves, J. Fluid Mech., 782, 25–36, doi:10.1017/jfm.2015.538, 2015.

Fedele, F., Brennan, J., Ponce de León, S., Dudley, J. and Dias, F.: Real world ocean rogue waves explained without the modulational instability., Sci. Rep., 6(1), 27715, doi:10.1038/srep27715, 2016.

Janssen, P. a. E. M.: On some consequences of the canonical transformation in the Hamiltonian theory of water waves, J. Fluid Mech., 637, 1–44, doi:10.1017/S0022112009008131, 2009.

Waseda, T., Kinoshita, T. and Tamura, H.: Evolution of a Random Directional Wave and Freak Wave Occurrence, J. Phys. Oceanogr., 39(3), 621–639, doi:10.1175/2008JPO4031.1, 2009.

West, B. J., Brueckner, K. A., Janda, R. S., Milder, D. M. and Milton, R. L.: A New numerical method 'for surface hydrodynamics, J. Geophys. Res. Ocean., 92(C11), 11803–11824, doi:10.1029/JC092iC11p11803, 1987.

Xiao, W., Liu, Y., Wu, G. and Yue, D. K. P.: Rogue wave occurrence and dynamics by direct simulations of nonlinear wave-field evolution, J. Fluid Mech., 720, 357–392, doi:10.1017/jfm.2013.37, 2013.